ACSNANO
www.acsnano.org

ARTICLE

Self-Powered Electrospinning System Driven by a Triboelectric Nanogenerator

Congju Li,*[,†] Yingying Yin,[†] Bin Wang,[‡] Tao Zhou,[†] Jiaona Wang,[‡] Jianjun Luo,[†] Wei Tang,[†] Ran Cao,[†] Zuqing Yuan,[†] Nianwu Li,[†] Xinyu Du,[†] Chunru Wang,*[,§] Shuyu Zhao,[‡] Yuebo Liu,[‡] and Zhong Lin Wang*[,†,∥]

[†]Beijing Institute of Nanoenergy and Nanosystems, Chinese Academy of Sciences, National Center for Nanoscience and Technology (NCNST), Beijing 100083, China

[‡]School of Materials Science & Engineering, Beijing Institute of Fashion Technology, Beijing 100029, China

[§]CAS Key Laboratory of Molecular Nanostructure and Nanotechnology, Institute of Chemistry, Chinese Academy of Science, Beijing 100190, China

[∥]School of Materials Science and Engineering, Georgia Institute of Technology, Atlanta, Georgia 30332-0245, United States

S *Supporting Information*

ABSTRACT: **Broadening the application area of the triboelectric nanogenerators (TENGs) is one of the research emphases in the study of the TENGs, whose output characteristic is high voltage with low current. Here we design a self-powered electrospinning system, which is composed of a rotating-disk TENG (R-TENG), a voltage-doubling rectifying circuit (VDRC), and a simple spinneret. The R-TENG can generate an alternating voltage up to 1400 V. By using a voltage-doubling rectifying circuit, a maximum constant direct voltage of 8.0 kV can be obtained under the optimal configuration and is able to power the electrospinning system for fabricating various polymer nanofibers, such as polyethylene terephthalate (PET), polyamide-6 (PA6), polyacrylonitrile (PAN), polyvinylidene difluoride (PVDF), and thermoplastic polyurethanes (TPU). The system demonstrates the capability of a TENG for high-voltage applications, such as manufacturing nanofibers by electrospinning.**

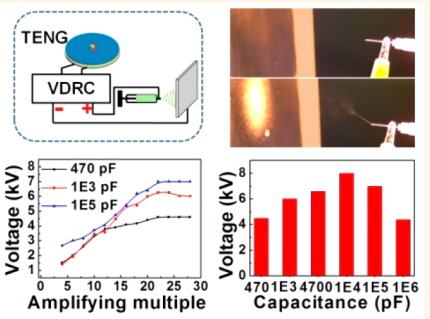

KEYWORDS: *triboelectric nanogenerator, electrospinning system, voltage-doubling rectifying circuit, high voltage, nanofibers*

Electrospinning is a powerful technique that uses an electrically forced fluid jet to form nanofibers from a polymer solution or melt.[1−3] Due to the high specific surface area and porosity,[4,5] electrospinning nanofibers have been extensively and maturely applied in drug delivery, tissue engineering, filtration, and sensors.[6−10] In the electrospinning process, the high voltage not only charges the polymer solution or melt at first but also assists the charged jet in overcoming the surface force to eject onto the receiver and plays a vital role in control of fiber morphology.[11,12] The high voltage used in the electrospinning process is usually provided by a DC power source with a voltage ranging from several to tens of kilovolts,[13] deeply dependent on the heavy hardware circuit and power system, which seriously restricted the application scenarios of electrospinning. Therefore, the development of an independent power source for electrospinning is highly desirable.

Different from piezoelectric nanogenerators,[14,15] the recently invented triboelectric nanogenerators (TENGs) are based on the triboelectrification and electrostatic induction,[16−18] which can convert various types of mechanical energy in our living environment into electricity.[19−21] By integrating with power management circuits, TENGs have been proved to be a promising sustainable power source in self-powered systems, such as self-charging power units based on biomechanical energy harvesting for wearable electronics,[22−24] self-powered human body motion sensors,[25,26] self-powered wastewater treatment,[27,28] and self-powered multifunctional sensors.[29] The output characteristic of the TENGs is high voltage with low current.[30,31] Therefore, transformers are usually used for driving low-voltage equipment by reducing the voltage while increasing the current.[32−35] However, many manufacturing equipment needs higher voltage than the output of the TENGs, with lower working current. Like electrospinning, the working voltage ranges from several to tens of kilovolts, while the working current is just several microamps.[13,36]

Here we report a self-powered electrospinning system, which is composed of a rotating-disk TENG (R-TENG), a voltage-doubling rectifying circuit (VDRC), and a simple spinneret. The rationally designed system can execute the electrospinning

Received: August 8, 2017
Accepted: September 19, 2017
Published: September 19, 2017

ACS Publications © XXXX American Chemical Society

DOI: 10.1021/acsnano.7b05626
ACS Nano XXXX, XXX, XXX−XXX

process without any external power source. The R-TENG works in the freestanding mode and can generate an alternating current with an open-circuit voltage (V_{OC}) of about 1400 V, a short-circuit current (I_{SC}) of about 5.5 mA, and maximum instantaneous power of 1.08 W on the optimum external load of 120 kΩ.[37] To actuate the electrospinning process, a VDRC was designed to obtain the desired high DC voltage. Under the optimal configuration, a maximum constant DC voltage of 8.0 kV can be obtained and is able to power the electrospinning system for fabricating various polymer nanofibers, such as PET, PA6, PAN, PVDF, and TPU. The system demonstrates the capability of TENGs for high-voltage applications, such as manufacturing nanofibers by electrospinning. All used materials are commercially available with low cost, and the entire electrospinning system is self-powered. Our study not only demonstrates the potential application of the TENGs in high-voltage manufacturing equipment but also broadens the application scenarios of electrospinning, especially in the field or in remote places without an electric power supply.

RESULTS AND DISCUSSION

Structural design and photographs of the self-powered electrospinning system are shown in Figure 1. The self-powered electrospinning system is composed of an energy harvesting and converting unit (R-TENG), a VDRC, and a simple spinneret, as shown in Figure 1a. The structural design of the R-TENG is shown in Figure 1b, which consists of three layers: a layer of radial-arrayed Cu strips (rotator) as one frictional material, a layer of fluorinated ethylene propylene (FEP) film (50 μm thickness) as another frictional material, and a layer of two sets of complementary radial-arrayed Cu strips (stator) as electrodes. Both of the Cu layers were prepared based on printed circuit board (PCB) technique (see Methods section for the detailed preparation process of the R-TENG). Figure 1c is a photograph of the rotator (left) and stator (right) of the R-TENG. Figure 1d is a photograph of the assembled hand-cranked R-TENG.

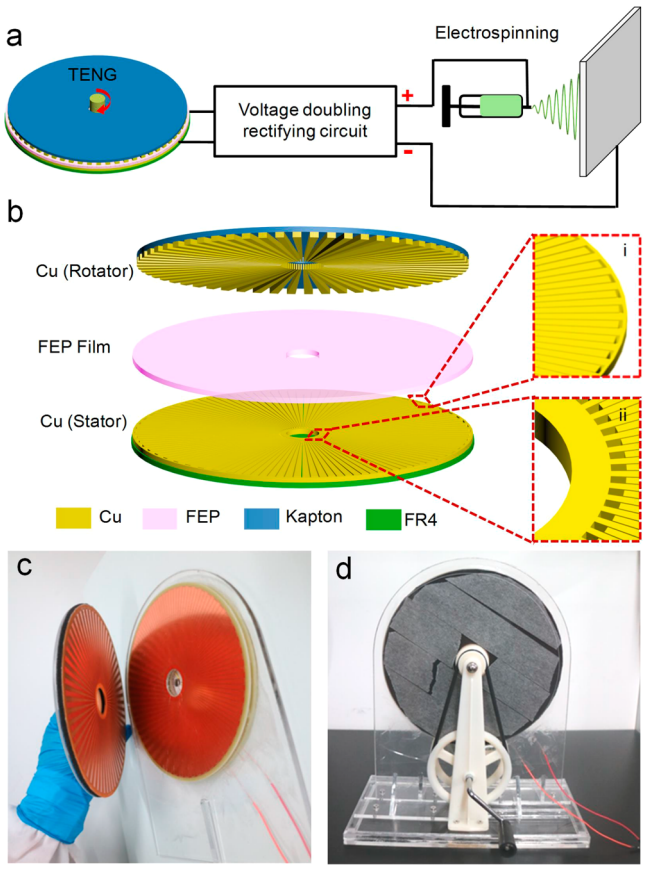

Figure 1. Structural design and photographs of the self-powered electrospinning system. (a) Schematic illustration of the self-powered electrospinning system. (b) Structural design of the R-TENG. (c) Photograph of the rotator and stator of the R-TENG. (d) Photograph of the hand-cranked R-TENG.

The working mechanism and electrical characterization of the R-TENG are shown in Figure 2. As shown in Figure 2a, the R-TENG works in the freestanding mode, and the electricity generation process can be divided into three stages: initial state, intermediate state, and final state.[37,38] As the top Cu layer (on the rotator) slides along the surface of the FEP film (on the stator), triboelectric charges will generate and distribute on their surfaces. The density of positive charges on Cu is twice as much as the negative charges on the FEP according to the law of charge conservation.[39] At the initial state, when the rotator is completely aligned with the left electrode, this electrode has negative charges and the adjacent right electrode has the same quantity of positive charges to keep an electrostatic equilibrium (Figure 2a (i)). As the top Cu layer slides to the right electrode, free electrons flow from the left electrode to the right electrode *via* the external load (Figure 2a (ii)). At the final state, when the rotator is completely aligned with the right electrode, the charge distribution is just opposite the initial state (Figure 2a (iii)). In the same way, when the top Cu layer keeps rotating, a reverse current would be generated, forming a periodically alternating current in the load.

To investigate the output performance of the R-TENG quantitatively, a rotary motor was used to drive the R-TENG. As shown in Figure 2b and c, the open-circuit voltage (V_{OC}) and the short-circuit current (I_{SC}) of the R-TENG reach up to about 1400 V and 5.5 mA, respectively. To investigate the maximum output power of the R-TENG, the load matching test was implemented as shown in Figure 2d. With the load resistance increasing, the current decreases, while the output power increases first and then decreases. When the external load resistance is up to 120 kΩ, the output instantaneous power reaches a maximum of 1.08 W. Figure 2e displays the charging curves of different capacitors (1000, 4700, and 10 000 pF) by the R-TENG through a bridge rectifier. The inset shows the charging circuit diagram. It could be seen that although a larger capacitor would take more charging time, all capacitors attain 800 V within a few seconds.

Obviously, because of the rotary freestanding mode with grating structure and the large size,[40,41] the output property of the R-TENG is excellent. However, the required voltage in the electrospinning process is a DC voltage ranging from several to tens of kilovolts. Hence, the R-TENG that generates an AC voltage with a peak value of 1400 V is apparently unable to actuate the electrospinning process. To solve this problem, a VDRC was designed. The working mechanism and electrical characterization of the VDRC are shown in Figure 3. Figure 3a shows the I_{SC} of the R-TENG in one cycle, and Figure 3b shows the circuit diagram of the VDRC, which is a regular arrangement of diodes and capacitors. It is worth noting that the VDRC works without an external power source. When the output current is in the positive periodic, diode D_1 is in the forward conducting state. The current flows through D_1 to

DOI: 10.1021/acsnano.7b05626
ACS Nano XXXX, XXX, XXX−XXX

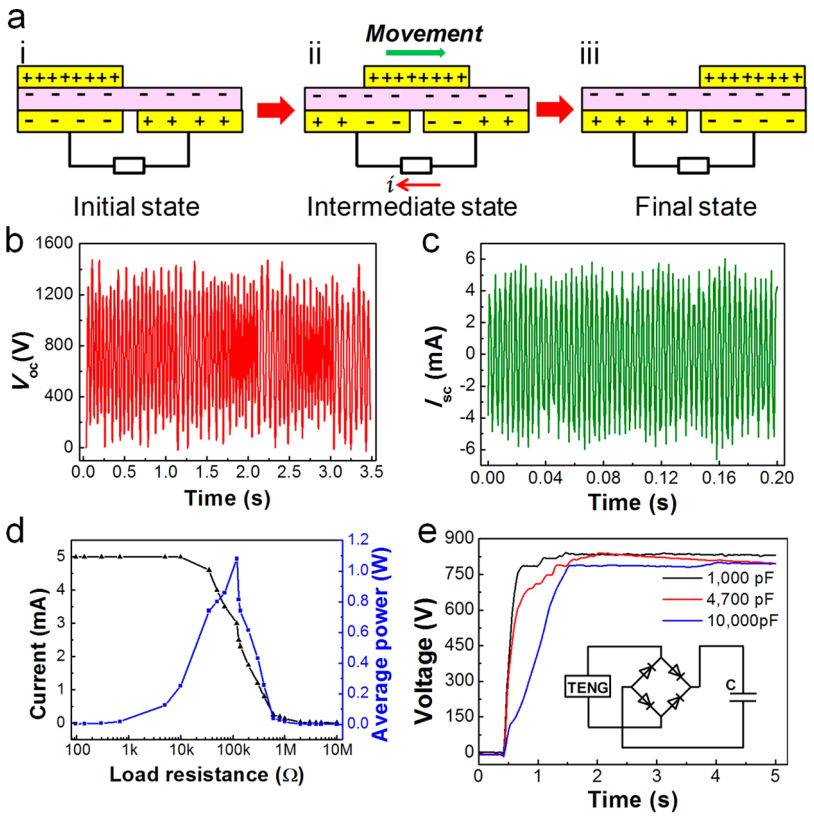

Figure 2. Working mechanism and electrical characterization of the R-TENG. (a) Schematic illustration of working principle of the R-TENG. (b) Open-circuit voltage (V_{OC}) of the R-TENG. (c) Short-circuit current (I_{SC}) of the R-TENG. (d) Dependence of the output current and instantaneous power of the R-TENG on the external load resistance. (e) Charging curves of different capacitors by the R-TENG through a bridge rectifier. Inset: Charging circuit diagram.

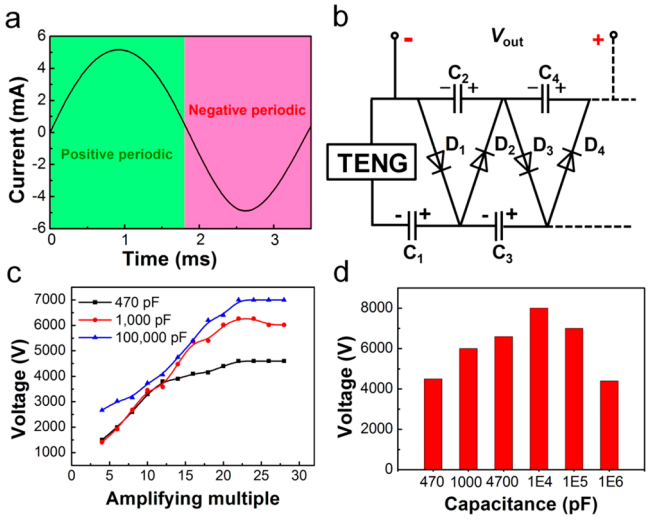

Figure 3. Working mechanism and electrical characterization of the voltage-doubling rectifying circuit (VDRC). (a) Output current of the R-TENG in one cycle. (b) Working mechanism of the VDRC. Output voltage of the VDRC (V_{out}) as a function of the (c) amplifying multiple and (d) capacitance value.

charge the capacitor C_1. In the ideal case, the voltage on C_1 (V_1) is equal to the output voltage of the R-TENG (V_{TENG}), with the cathode on the left while the anode is on the opposite side. When the current is in the negative periodic, D_1 is in the reverse blocking state, while D_2 is in the forward conducting state. The current flows through D_2 to charge the capacitor C_2. Based on Kirchhoff voltage laws (KVL), V_2 is doubled compared with V_{TENG}, with the cathode on the left while the anode is on the opposite side. Similarly, when the current is in the positive periodic again, C_3 is charged to V_3, which is 2 times bigger than V_{TENG}, with the cathode on the left while the anode is on the opposite side. Thus, if more couples of diodes and capacitors were added in the circuit, after undergoing several periods, charging capacitors repeatedly, every capacitor (except C_1) would be charged to $2V_{TENG}$, with the cathode on left while the anode is on the opposite side. Therefore, at the two ends of the capacitor pack, multiple DC will be gained finally.

In the actual situation, the V_{out} (two end sides voltage of the top capacitor pack, Figure 3b) could not reach the theoretical value due to the ohmic loss and the limited output power of the R-TENG. Therefore, the relationship between V_{out} and the amplifying multiple was investigated with the R-TENG as the power supply. Here, the "amplifying multiple" is the theoretical magnification of the V_{TENG}, which is determined by the number of diodes and capacitors in the circuit. For different capacitance values, with the increase of the amplifying multiple, all the V_{out} increase first and then keep steady (Figure 3c). It could be seen that 22 is the optimal magnification in this work, which generates output voltages of 7.0, 6.3, and 4.6 kV for different capacitance values of 100 000, 1000, and 470 pF, respectively. It also indicates that the capacitance value plays an important role in the final V_{out}. The V_{out} values under an optimized amplifying multiple of 22 with various capacitance values were measured to obtain the optimal output (Figure 3d). In the ideal case, as long as the withstand voltage of the capacitor is higher than $2V_{TENG}$, the capacitance value has no effect on the final V_{out}. But in fact,

DOI: 10.1021/acsnano.7b05626
ACS Nano XXXX, XXX, XXX−XXX

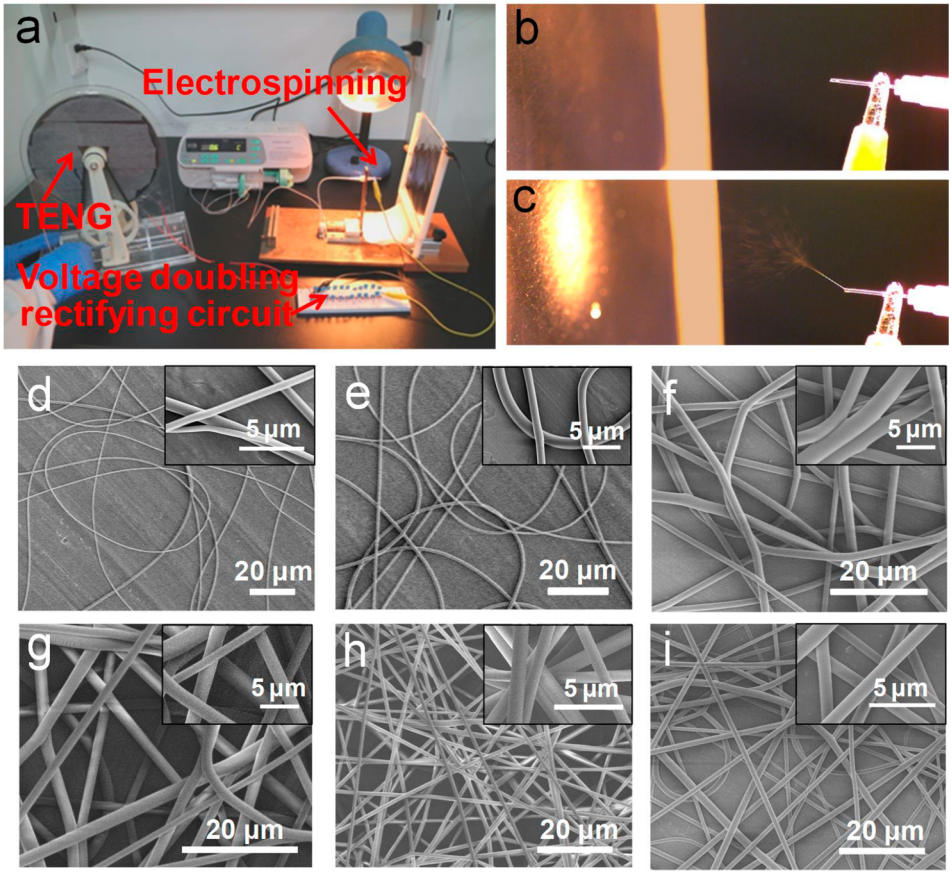

Figure 4. Performance of the self-powered electrospinning system under different amplifying multiples. (a) Photograph of the self-powered electrospinning system. (b, c) High-speed photographs of the needle before and after the rotation of the R-TENG. (d–i) SEM images of the PET nanofibers fabricated under an amplifying multiple of 6, 8, 10, 16, 22, and 28, respectively, where the capacitance value in the VDRC is chosen as 1×10^5 pF. Insets: Enlarged view of the PET nanofibers.

as shown in Figure 3d, the V_{out} increases first and then decreases with the increase of the capacitance value. This is because the output power of the R-TENG is limited, which determines the final V_{out}. As shown in Figure 2d, the output power reaches the maximum output power with the matched external load. For the VDRC, different capacitance values mean different external loads of the R-TENG. We conclude that when the capacitance value is 1×10^4 pF, the equivalent load of the VDRC is close to the matched external load of the R-TENG. Therefore, the maximum V_{out} of 8.0 kV can be obtained with the optimized conditions (capacitance value, 1×10^4 pF; amplifying multiple, 22).

We investigated the performance of the self-powered electrospinning system under different configurations, *i.e.*, the amplifying multiple and the capacitance value. The influence of the amplifying multiple is presented in Figure 4, where the capacitance value is 100 000 (1×10^5) pF. A photograph of the self-powered electrospinning system is shown in Figure 4a. In this experiment, polyethylene terephthalate (PET) was chosen as the electrospinning solution because it is a widely used polymer material with good physical and mechanical properties, is acid and alkali resistant, and has fatigue durability and dimensional stability.[42] Before the electrospinning process, the PET solution was loaded in a syringe connected with a needle tip, and the positive electrode of the V_{out} was connected to the needle tip as well. A piece of aluminum foil was connected to the negative electrode of the V_{out} to collect the electrospun nanofibers (see Methods section for the detailed preparation of the electrospinning process). When the amplifying multiple is 22, a Taylor cone is triggered by the R-TENG, fabricating plenty of PET nanofibers on the Al foil. Figure 4b and c are photographs of the needle before and after the rotation of the R-TENG. Since the amplifying multiple has a defining impact on the V_{out}, it will greatly influence the amount and morphology of the PET nanofibers. Figure 4d–i are the SEM images of the PET nanofibers fabricated under amplifying multiples of 6, 8, 10, 16, 22, and 28, respectively. The insets are enlarged views of the PET nanofibers. During the course of the experiment, we observed that consecutive Taylor cone will be triggered only when the V_{out} is higher than a certain value. The critical voltage for PET is 5.0 kV, which was measured by a commercial electrospinning equipment. When the V_{out} is lower than 5.0 kV, intermittent nanofibers can be triggered and the obtained nanofibers are sparse, as shown in Figure 4d (3.0 kV), Figure 4e (3.2 kV), and Figure 4f (3.7 kV). Due to the lack of sufficient stretch under lower voltage, we can see that the nanofibers are bent and some of them are intertwined with each other. When the V_{out} is higher than 5.0 kV, the distribution of nanofibers is dense and uniform, as shown in Figure 4g (5.4 kV), Figure 4h (7.0 kV), and Figure 4i (7.0 kV). The nanofibers are straightened under the higher electrostatic force. Theoretically, the diameter of nanofibers decreases with the increase of voltage. But the change is not evident here because the voltage has only a slight increase.[43] It could be seen that when the amplifying multiple is larger than 22, the fabricated PET nanofibers are abundant with good shape.

DOI: 10.1021/acsnano.7b05626
ACS Nano XXXX, XXX, XXX–XXX

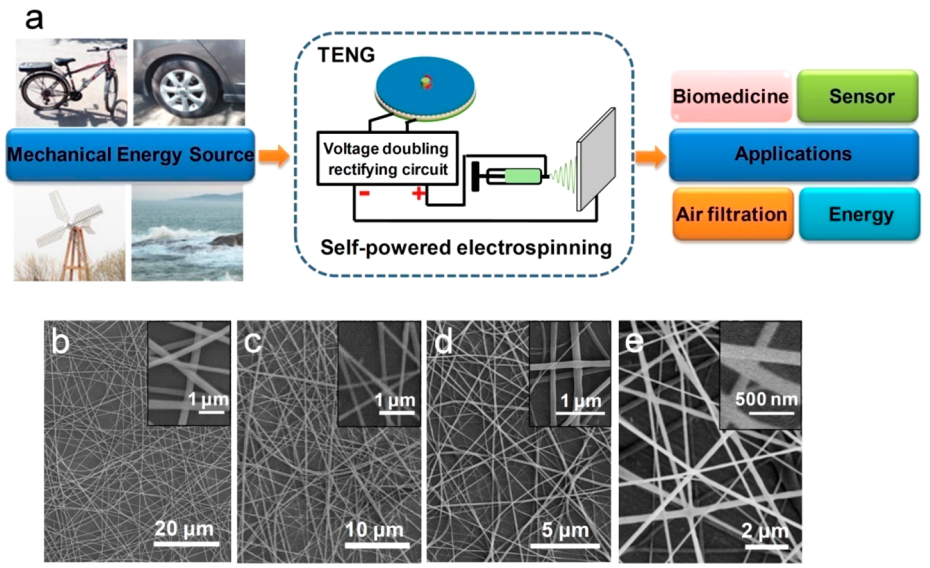

Figure 5. Potential applications of the self-powered electrospinning system. (a) System diagram of the self-powered electrospinning system. (b) PA6, (c) PAN, (d) PVDF, and (e) TPU nanofibers fabricated by the system under the amplifying multiple of 22 and capacitance value of 1 × 10^5 pF.

The influence of the capacitance value is presented in Figure S1 (Supporting Information), where the amplifying multiple is set as 22. Figure S1a–f (Supporting Information) are the SEM images of the PET nanofibers fabricated under different capacitance values (470, 1000, 4700, 1 × 10^4, 1 × 10^5, and 1 × 10^6 pF), respectively. The insets are the enlarged view of the PET nanofibers. It could be seen that the amount and morphology of the PET nanofibers are excellent when the capacitance value ranges from 1 × 10^4 to 1 × 10^5 pF. When the capacitance value is too small, the charges stored in the capacitors are not enough to guarantee a continuous electrospinning process. On the contrary, when the capacitance value is too large, the VDRC will take a long time to achieve the required high voltage. Based on the above analysis, it could be concluded that the optimum configuration is obtained under the amplifying multiple of 22 and capacitance value ranging from 1 × 10^4 to 1 × 10^5 pF.

The electrospinning process of PET was recorded by a high-speed camera (Movie S1, Supporting Information) and normal digital camera (Movie S2, Supporting Information). To shoot the whole charging and electrospinning process by a normal digital camera, the R-TENG was operated by a rotary motor at a rotation rate of 1200 rpm. A consecutive Taylor cone was triggered by the system within 5 s after the operation of the R-TENG. This continuous electrospinning process can also be triggered by hand rotating within several minutes.

Figure S2a (Supporting Information) is the SEM image of the PET nanofibers fabricated by the self-powered electrospinning system under an amplifying multiple of 22 and capacitance value of 1 × 10^5 pF. Figure S2b (Supporting Information) is the SEM image of the PET nanofibers fabricated by commercial electrospinning equipment under a voltage of 7 kV. It reveals that the nanofiber prepared by the self-powered electrospinning system is comparable in quality to that fabricated using a commercial electrospinning machine.

As shown in Figure 5, the introduction of the R-TENG made it possible to harvest various kinds of mechanical energy. In addition to PET nanofibers, the system is capable of manufacturing various nanofibers that require a high voltage less than 8.0 kV. Figure 5b–e are the SEM images of the PA6, PAN, PVDF, and TPU nanofibers fabricated by the system under an amplifying multiple of 22 and capacitance value of 1 × 10^5 pF, which demonstrates the feasibility of the self-powered electrospinning system.

CONCLUSION

In summary, the self-powered electrospinning system driven by a TENG is achieved by the combination of an R-TENG, a voltage-doubling rectifying circuit, and a simple spinneret. To actuate the electrospinning process by the R-TENG, a VDRC is designed and systematically investigated to obtain the optimum configuration. Finally, under an amplifying multiple of 22 and capacitance value of 1 × 10^4 pF, the system can output a maximum constant DC voltage of 8.0 kV. The self-powered electrospinning system exhibits excellent performance in the manufacturing of various polymer nanofibers, such as PET, PA6, PAN, PVDF, and TPU.

The self-powered electrospinning system driven by the R-TENG is comparable with commercial electrospinning machines and has the merits of simple structure, low cost, light weight, high efficiency, and energy conservation, which will bring a great breakthrough to the electrospinning technique, especially in the field or in remote places without an electric power supply. Typically, it has been proved that polymer nanofibers can be directly spun onto the injured location of skin to form a fibrous mat, which can not only prevent bacteria from entering the wound but also allow skin to breathe.[11] The wound therapy does not need too many nanofibers. It is feasible to treat skin wounds through short-time, even intermittent electrospinning. Therefore, the self-powered electrospinning system may have great potential applications in wilderness therapy by laborious work in turn. With an appropriate power management circuit, the TENG can not only be used for powering low-voltage electronics but also be applied for powering high-voltage manufacturing equipment.

DOI: 10.1021/acsnano.7b05626
ACS Nano XXXX, XXX, XXX–XXX

METHODS

Preparation Process of R-TENG. The rotator of the R-TENG is a collection of radial-arrayed Cu strips with a unit central angle of 3°, the same as the center angles of intervals. Every complementary arrayed sector in the stator is 3° with fine trenches between each other. As shown in the inset of Figure 1b, one kind of sector is connected at the outer ring, while the other kind of sector is connected at the inner ring, forming two complementary electrodes. The substrates of the rotator and stator are different, with flexible Kapton (100 μm thickness) for the rotator and stiff glass epoxy (FR4, 2 mm thickness) for the stator. The inner and outer diameters are 40 mm and 300 mm, respectively, for both of them. Finally, the stator and rotator of the R-TENG are installed onto a self-designed plastic fixture with a foam layer (4 mm thickness) attached onto the rotator as a buffer to ensure intimate contact between them.

Preparation of the Electrospinning Process. The solution systems of the polymers used in the present work include a 12 wt % of PET in a mixed solution of dichloromethane (DCM) and trifluoroacetic acid (TFA) with a volume ratio of 1:4, 14 wt % of PA6 in formic acid, 11 wt % of PAN in dimethylformamide (DMF), 10 wt % of PVDF in a mixed solution of DMF and acetone with a volume ratio of 7:3, and 21 wt % of TPU in a mixed solution of DMF and DCM with a volume ratio of 5:1. Then, the electrospinning solution was loaded in a 10 mL syringe with a 24-gauge needle tip, which was connected to the positive electrode of the V_{out}. The solution was pumped out of the needle tip using a syringe pump with an injection rate of 0.3 mL/h. A piece of aluminum foil was connected to the negative electrode of the V_{out} to collect the electrospun nanofibers, with a tip-to-collector distance of 5.5 cm. An electric heating lamp was utilized in the whole electrospinning process.

Electrical Measurement and Characterization. The I_{SC} was measured by an electrometer (Keithley, 6514) that has a fast response time (can record 1000 points per second) to monitor the real-time changes of I_{SC} at the rotation rate of 1200 rpm. But the V_{OC} was far beyond the detecting range of the electrometer. So the V_{OC} was measured by a noncontacting electrostatic probe (Trek-347), whose response time is less than 3 ms for a 1000 V step. Before measuring, one end of the V_{OC} was grounded, while the other end was connected with a Cu film that was placed below the probe at a distance of 3 mm. This slow response time cannot monitor the real-time changes of V_{OC} at the rotation rate of 1200 rpm. A large number of studies have proved that the amplitude of V_{OC} remains stable regardless of the rotation rate.[39] So we measured the V_{OC} at the rotation rate of 100 rpm. The V_{out} was also obtained by the noncontacting electrostatic probe (Trek-347). The R-TENG was operated by a rotary motor (PC Motor, 6IK180RGU-CF). The morphology of the as-prepared polymer nanofibers was characterized by a Hitachi SU8020 field emission scanning electron microscope, operated at 5 kV and 10 μA.

ASSOCIATED CONTENT

Supporting Information

The Supporting Information is available free of charge on the ACS Publications website at DOI: 10.1021/acsnano.7b05626.

Figures providing photographs of the performance of the self-powered electrospinning system with different capacitance values; comparison of the self-powered electrospinning system with commercial electrospinning power source (PDF)

Movie S1: electrospinning process of PET recorded by a high-speed camera (AVI)

Movie S2: electrospinning process of PET recorded by a normal digital camera (AVI)

AUTHOR INFORMATION

Corresponding Authors

*E-mail: licongju@binn.cas.cn.

*E-mail: crwang@iccas.ac.cn.

*E-mail: zlwang@gatech.edu.

ORCID

Congju Li: 0000-0001-6030-7002

Zuqing Yuan: 0000-0003-3988-0618

Xinyu Du: 0000-0003-1101-7409

Chunru Wang: 0000-0001-7984-6639

Zhong Lin Wang: 0000-0002-5530-0380

Notes

The authors declare no competing financial interest.

ACKNOWLEDGMENTS

The authors are thankful for support from the National Key R&D Project from the Minister of Science and Technology, China (2016YFA0202702), the Natural Science Foundation of China (NSFC Nos. 21274006 and 51503005), the Programs for Beijing Science and Technology Leading Talent (Grant No. Z16111000490000), and the "Thousands Talents" Program for Pioneer Researcher and His Innovation Team, China.

REFERENCES

(1) Bellan, L. M.; Craighead, H. G. Nanomanufacturing Using Electrospinning. *Journal of Manufacturing Science and Engineering* **2009**, *131*, 034001.

(2) Li, D.; Xia, Y. Electrospinning of Nanofibers: Reinventing the Wheel? *Adv. Mater.* **2004**, *16*, 1151−1170.

(3) Bhardwaj, N.; Kundu, S. C. Electrospinning: A Fascinating Fiber Fabrication Technique. *Biotechnol. Adv.* **2010**, *28*, 325−347.

(4) Rose, M.; Kockrick, E.; Senkovska, I.; Kaskel, S. High Surface Area Carbide-Derived Carbon Fibers Produced by Electrospinning of Polycarbosilane Precursors. *Carbon* **2010**, *48*, 403−407.

(5) Choong, L. T.; Khan, Z.; Rutledge, G. C. Permeability of Electrospun Fiber Mats under Hydraulic Flow. *J. Membr. Sci.* **2014**, *451*, 111−116.

(6) Cho, J. S.; Hong, Y. J.; Kang, Y. C. Design and Synthesis of Bubble-Nanorod-Structured Fe_2O_3-Carbon Nanofibers as Advanced Anode Material for Li-Ion Batteries. *ACS Nano* **2015**, *9*, 4026−4035.

(7) Sridhar, R.; Lakshminarayanan, R.; Madhaiyan, K.; Amutha Barathi, V.; Lim, K. H.; Ramakrishna, S. Electrosprayed Nanoparticles and Electrospun Nanofibers Based on Natural Materials: Applications in Tissue Regeneration, Drug Delivery and Pharmaceuticals. *Chem. Soc. Rev.* **2015**, *44*, 790−814.

(8) Hu, X.; Liu, S.; Zhou, G.; Huang, Y.; Xie, Z.; Jing, X. Electrospinning of Polymeric Nanofibers for Drug Delivery Applications. *J. Controlled Release* **2014**, *185*, 12−21.

(9) Strain, I. N.; Wu, Q.; Pourrahimi, A. M.; Hedenqvist, M. S.; Olsson, R. T.; Andersson, R. L. Electrospinning of Recycled PET to Generate Tough Mesomorphic Fibre Membranes for Smoke Filtration. *J. Mater. Chem. A* **2015**, *3*, 1632−1640.

(10) Li, W.; Ma, S.; Li, Y.; Yang, G.; Mao, Y.; Luo, J.; Gengzang, D.; Xu, X.; Yan, S. Enhanced Ethanol Sensing Performance of Hollow ZnO−SnO_2 Core−Shell Nanofibers. *Sens. Actuators, B* **2015**, *211*, 392−402.

(11) Huang, Z.-M.; Zhang, Y. Z.; Kotaki, M.; Ramakrishna, S. A Review on Polymer Nanofibers by Electrospinning and Their Applications in Nanocomposites. *Compos. Sci. Technol.* **2003**, *63*, 2223−2253.

(12) Deitzel, J. M.; Kleinmeyer, J.; Harris, D.; Tan, N. C. B. The Effect of Processing Variables on the Morphology of Electrospun Nanofibers and Textiles. *Polymer* **2001**, *42*, 261−272.

(13) Lu, X.; Wang, C.; Favier, F.; Pinna, N. Electrospun Nanomaterials for Supercapacitor Electrodes: Designed Architectures and Electrochemical Performance. *Adv. Energy Mater.* **2017**, *7*, 1601301.

DOI: 10.1021/acsnano.7b05626
ACS Nano XXXX, XXX, XXX−XXX

(14) Zhang, Y.; Yan, X.; Yang, Y.; Huang, Y.; Liao, Q.; Qi, J. Scanning Probe Study on the Piezotronic Effect in ZnO Nanomaterials and Nanodevices. *Adv. Mater.* **2012**, *24*, 4647−4655.
(15) Zhang, Y.; Yang, Y.; Gu, Y.; Yan, X.; Liao, Q.; Li, P.; Zhang, Z.; Wang, Z. Performance and Service Behavior in 1-D Nanostructured Energy Conversion Devices. *Nano Energy* **2015**, *14*, 30−48.
(16) Wang, Z. L. Triboelectric Nanogenerators as New Energy Technology for Self-Powered Systems and as Active Mechanical and Chemical Sensors. *ACS Nano* **2013**, *7*, 9533−9557.
(17) Xie, Y.; Wang, S.; Niu, S.; Lin, L.; Jing, Q.; Yang, J.; Wu, Z.; Wang, Z. L. Grating-Structured Freestanding Triboelectric-Layer Nanogenerator for Harvesting Mechanical Energy at 85% Total Conversion Efficiency. *Adv. Mater.* **2014**, *26*, 6599−6607.
(18) Jiang, T.; Zhang, L. M.; Chen, X.; Han, C. B.; Tang, W.; Zhang, C.; Xu, L.; Wang, Z. L. Structural Optimization of Triboelectric Nanogenerator for Harvesting Water Wave Energy. *ACS Nano* **2015**, *9*, 12562−12572.
(19) Wen, X.; Yang, W.; Jing, Q.; Wang, Z. L. Harvesting Broadband Kinetic Impact Energy from Mechanical Triggering/Vibration and Water Waves. *ACS Nano* **2014**, *8*, 7405−7412.
(20) Wang, X.; Niu, S.; Yi, F.; Yin, Y.; Hao, C.; Dai, K.; Zhang, Y.; You, Z.; Wang, Z. L. Harvesting Ambient Vibration Energy over a Wide Frequency Range for Self-Powered Electronics. *ACS Nano* **2017**, *11*, 1728−1735.
(21) Lin, L.; Wang, S.; Xie, Y.; Jing, Q.; Niu, S.; Hu, Y.; Wang, Z. L. Segmentally Structured Disk Triboelectric Nanogenerator for Harvesting Rotational Mechanical Energy. *Nano Lett.* **2013**, *13*, 2916−2923.
(22) Pu, X.; Li, L.; Song, H.; Du, C.; Zhao, Z.; Jiang, C.; Cao, G.; Hu, W.; Wang, Z. L. A Self-Charging Power Unit by Integration of a Textile Triboelectric Nanogenerator and a Flexible Lithium-Ion Battery for Wearable Electronics. *Adv. Mater.* **2015**, *27*, 2472−2478.
(23) Kuang, S. Y.; Chen, J.; Cheng, X. B.; Zhu, G.; Wang, Z. L. Two-Dimensional Rotary Triboelectric Nanogenerator as a Portable and Wearable Power Source for Electronics. *Nano Energy* **2015**, *17*, 10−16.
(24) Zhu, G.; Peng, B.; Chen, J.; Jing, Q.; Lin Wang, Z. Triboelectric Nanogenerators as a New Energy Technology: From Fundamentals, Devices, to Applications. *Nano Energy* **2015**, *14*, 126−138.
(25) Zhang, Q.; Liang, Q.; Liao, Q.; Yi, F.; Zheng, X.; Ma, M.; Gao, F.; Zhang, Y. Service Behavior of Multifunctional Triboelectric Nanogenerators. *Adv. Mater.* **2017**, *29*, 1606703.
(26) Yi, F.; Wang, X.; Niu, S.; Li, S.; Yin, Y.; Dai, K.; Zhang, G.; Lin, L.; Wen, Z.; Guo, H.; et al. A Highly Shape-Adaptive, Stretchable Design Based on Conductive Liquid for Energy Harvesting and Self-Powered Biomechanical Monitoring. *Sci. Adv.* **2016**, *2* (6), e1501624.
(27) Jiang, Q.; Jie, Y.; Han, Y.; Gao, C.; Zhu, H.; Willander, M.; Zhang, X.; Cao, X. Self-Powered Electrochemical Water Treatment System for Sterilization and Algae Removal Using Water Wave Energy. *Nano Energy* **2015**, *18*, 81−88.
(28) Li, Z.; Chen, J.; Guo, H.; Fan, X.; Wen, Z.; Yeh, M. H.; Yu, C.; Cao, X.; Wang, Z. L. Triboelectrification-Enabled Self-Powered Detection and Removal of Heavy Metal Ions in Wastewater. *Adv. Mater.* **2016**, *28*, 2983−2991.
(29) Ma, M.; Liao, Q.; Zhang, G.; Zhang, Z.; Liang, Q.; Zhang, Y. Self-Recovering Triboelectric Nanogenerator as Active Multifunctional Sensors. *Adv. Funct. Mater.* **2015**, *25*, 6489−6494.
(30) Wang, H. S.; Jeong, C. K.; Seo, M.-H.; Joe, D. J.; Han, J. H.; Yoon, J.-B.; Lee, K. J. Performance-Enhanced Triboelectric Nanogenerator Enabled by Wafer-Scale Nanogrates of Multistep Pattern Downscaling. *Nano Energy* **2017**, *35*, 415−423.
(31) Seol, M.-L.; Han, J.-W.; Park, S.-J.; Jeon, S.-B.; Choi, Y.-K. Hybrid Energy Harvester with Simultaneous Triboelectric and Electromagnetic Generation from an Embedded Floating Oscillator in a Single Package. *Nano Energy* **2016**, *23*, 50−59.
(32) Guo, H.; Wen, Z.; Zi, Y.; Yeh, M.-H.; Wang, J.; Zhu, L.; Hu, C.; Wang, Z. L. A Water-Proof Triboelectric-Electromagnetic Hybrid Generator for Energy Harvesting in Harsh Environments. *Adv. Energy Mater.* **2016**, *6*, 1501593.
(33) Xi, F.; Pang, Y.; Li, W.; Jiang, T.; Zhang, L.; Guo, T.; Liu, G.; Zhang, C.; Wang, Z. L. Universal Power Management Strategy for Triboelectric Nanogenerator. *Nano Energy* **2017**, *37*, 168−176.
(34) Moon, H.; Chung, J.; Kim, B.; Yong, H.; Kim, T.; Lee, S.; Lee, S. Stack/Flutter-Driven Self-Retracting Triboelectric Nanogenerator for Portable Electronics. *Nano Energy* **2017**, *31*, 525−532.
(35) Wang, S.; Lin, L.; Wang, Z. L. Nanoscale Triboelectric-Effect-Enabled Energy Conversion for Sustainably Powering Portable Electronics. *Nano Lett.* **2012**, *12*, 6339−6346.
(36) Yalcinkaya, B.; Yener, F.; Jirsak, O.; Cengiz-Callioglu, F. On the Nature of Electric Current in the Electrospinning Process. *J. Nanomater.* **2013**, *2013*, 1−10.
(37) Zi, Y.; Niu, S.; Wang, J.; Wen, Z.; Tang, W.; Wang, Z. L. Standards and Figure-of-Merits for Quantifying the Performance of Triboelectric Nanogenerators. *Nat. Commun.* **2015**, *6*, 8376.
(38) Jiang, T.; Chen, X.; Han, C. B.; Tang, W.; Wang, Z. L. Theoretical Study of Rotary Freestanding Triboelectric Nanogenerators. *Adv. Funct. Mater.* **2015**, *25*, 2928−2938.
(39) Zhu, G.; Chen, J.; Zhang, T.; Jing, Q.; Wang, Z. L. Radial-Arrayed Rotary Electrification for High Performance Triboelectric Generator. *Nat. Commun.* **2014**, *5*, 3426.
(40) Han, C.; Zhang, C.; Tang, W.; Li, X.; Wang, Z. L. High Power Triboelectric Nanogenerator Based on Printed Circuit Board (PCB) Technology. *Nano Res.* **2015**, *8*, 722−730.
(41) Chen, S.; Gao, C.; Tang, W.; Zhu, H.; Han, Y.; Jiang, Q.; Li, T.; Cao, X.; Wang, Z. Self-Powered Cleaning of Air Pollution by Wind Driven Triboelectric Nanogenerator. *Nano Energy* **2015**, *14*, 217−225.
(42) Cai, Y.; Ke, H.; Dong, J.; Wei, Q.; Lin, J.; Zhao, Y.; Song, L.; Hu, Y.; Huang, F.; Gao, W.; et al. Effects of Nano-SiO_2 on Morphology, Thermal Energy Storage, Thermal Stability, and Combustion Properties of Electrospun Lauric Acid/PET Ultrafine Composite Fibers as Form-Stable Phase Change Materials. *Appl. Energy* **2011**, *88*, 2106−2112.
(43) Lee, K. H.; Kim, H. Y.; La, Y. M.; Lee, D. R.; Sung, N. H. Influence of a Mixing Solvent with Tetrahydrofuran and N,N-Dimethylformamide on Electrospun Poly(vinyl chloride) Nonwoven Mats. *J. Polym. Sci., Part B: Polym. Phys.* **2002**, *40*, 2259−2268.

DOI: 10.1021/acsnano.7b05626
ACS Nano XXXX, XXX, XXX−XXX